On the interplay between Si-Er-O segregation and erbium silicate (Er 2 Si 2 O 7) formation in Er-doped SiO x thin films

Georges Beainy, C. Frilay, Philippe Pareige, F. Gourbilleau, Etienne Talbot

On the interplay between Si-Er-O segregation and erbium silicate ($Er_2Si_2O_7$) formation in Er-doped SiO_x thin films

G. Beainy [a], C. Frilay [b], P. Pareige [a], F. Gourbilleau [b], E. Talbot [a,*]

[a] Normandie Univ, UNIROUEN, INSA Rouen, CNRS, Groupe de Physique des Mat´eriaux, 76000, Rouen France,
[b] CIMAP, Normandie Univ, ENSICAEN, UNICAEN, CEA, CNRS, CIMAP, 14000, Caen, France

Keywords:
Nanostructured materials,
Oxide materials,
Rare earth alloys and compounds,
Semiconductors,
Atomic scale structure,
Optical properties Luminescence,
Atom probe tomography.

A B S T R A C T

Er-doped silica or rich-silicon oxide has been widely studied as 1.54 μm emitters. The incorporation of Si-nanoclusters is known for improving luminescence yield of Er^{3+} ions through an efficient sensitization of the neighboring rare earth ions. The aim of this work is to investigate the influence of Silicon excess and Erbium concentration on the formation of silicon nanoclusters and Er-rich phase responsible of the quenching of 1.54 μm emission. Atom probe tomography and photoluminescence spectroscopy were used to explore the nanostructure and optical activity of Er-doped silicon rich silica. We present a direct evidence that both silicon excess and Er concentration influence the growth of Si nanoclusters, the formation of Er-Si-O phase and the luminescence of both Si nanoclusters and Er^{3+} ions. We explain these finding in relation with the growth mechanism of nanoparticles and the presence of a Snowman-like Janus morphology between silicon and Erbium silicates nanoparticles. In this contribution, we deciphered the nanoscale structure spatial correlations between Er and Si atoms in Er doped SiO_X which remained unclear for a long time.

1. Introduction

The particular 1.54 μm emission wavelength of erbium (Er) has led to the development of Er-doped silica (SiO_2) fiber amplifiers that have made long-distance optical communication possible [1]. However, the weak absorption cross-section of Er-ions in SiO_2 ($\sim 10^{-20}$ cm^{-2}) requires high-power resonant excitation and further limits its application in miniaturized devices. An alternative approach to overcome this constraint is through the introduction of silicon nanoclusters (Si-ncs) within Er-doped SiO_2 [2,3]. The incorporation of Si-ncs improves the luminescence yield of Er^{3+} ions through an efficient sensitization of the neighboring Er^{3+} ions [4]. Er-doped silicon-rich silicon oxide (SRSO) is the most prevalent approach to obtain Si-ncs sensitizers and thus has aroused great interest during the last decade [2,5]. In this system, the variation in size or density of the Si-ncs, the content of Er, or the distance between Si-ncs and Er ions are crucial parameters that disturb the energy transfer efficiency and thus, the Er^{3+} luminescence. Moreover, the low solubility limit of Er ions in silicon oxide imposes major limitation. When Er content exceeds a critical modest concentration (10^{19} at cm^{-3}) [6], Er^{3+} ions will precipitate through clustering or formation of compounds such as oxides [6,7]. In many cases, these precipitates are responsible of emission deterioration, limiting thereby the progress of the optical properties of the system.

After two decades of research on the emission of Er^{3+} ions at 1.54 μm in SRSO, several issues remain unclear and still have to be deciphered. Indeed, the nature and the variation of the phases responsible for luminescence changes are still poorly understood, especially for high doping concentrations ($> 1-2$ at.%). Moreover, many questions persist about the spatial localization of the optically active Er^{3+} ions with respect to the Si nanoparticles. Specifically, either these ions are uniformly distributed, or they form agglomerates [8]. Therefore, mapping the Si and Er atoms distribution and the phase present in the sample with respect to elaboration and heat treatment conditions are key issues in controlling the required emission properties of such systems.

In this paper, we attempt to shed light on these fundamental aspects via an alternative approach of characterization of such system by performing 3D atom probe tomography (APT). Our overall objective is to monitor the nanoscale structure transformation of Si and Er nanoclusters and to explore their spatial

* Corresponding author.
E-mail address: etienne.talbot@univ-rouen.fr (E. Talbot).

correlations upon heat treatment. The present work leads to a comprehensive study of phase transformation occurring in highly Er-doped SiO_X thin films.

2. Experimental section

Er-doped SRSO layers were deposited on (100) oriented silicon wafer by magnetron co-sputtering of three confocal targets. The Si excess and Er content were independently tuned through the monitoring of the RF power applied on each cathode. The layers were grown at 500°C substrate temperature and 3 mTorr chamber pressure. Only Si excess and Er content have been modified to assess their respective consequences. The deposited layers were submitted to annealing treatments for 1 h under a nitrogen flux up to 1100°C to form the Si-ncs required for sensitization of Er^{3+} ions. More details on the fabrication conditions can be found elsewhere [9]. APT experiments were performed using a LAWATAP-CAMECA using UV (343 nm) femtosecond laser pulses (350 fs). A detailed description of this technique can be found in Lefebvre-Ulrikson et al. [10]. The photoluminescence properties were examined using a 476-nm excitation wavelength, which is non resonant for Er^{3+} ions, and always used to ensure the excitation of Er^{3+} by sensitization with Si-ncs.

3. Results and discussion

3.1. Elementary distribution of atoms

Table 1 reports the composition of the three analyzed samples measured by atom probe tomography. The measured composition of all species is constant over all the analyzed volume. The samples are labeled according to their silicon excess content.

The elementary distributions of Si and Er atoms, extracted from the APT analyzed volume on as-grown samples $Si_{4\%}$, $Si_{9\%}$, and $Si_{16\%}$ are shown in Fig. 1. For sample $Si_{4\%}$ (Fig. 1a), Si and Er atoms are randomly distributed as confirmed by the statistical test proposed by Thuvander et al. [11] (not shown here). However, this is obviously not the case for sample $Si_{16\%}$ (Fig. 1c), containing approximately the same Er content as the sample $Si_{4\%}$ (1.9 at.%) but primarily higher Si excess. Mappings noticeably show areas richer in Si and Er than others. For sample $Si_{9\%}$ (Fig. 1b), Er and Si rich areas are also observed but seem to be less highlighted than for sample $Si_{16\%}$. Besides, we find that the morphology of the areas rich in Si and Er is not yet well defined and has no distinct interface with the SRSO matrix of as-grown samples. Especially for sample $Si_{16\%}$, where a careful exploration of the mapping reveals that the rich areas are not well isolated but seem interconnected. These outcomes indicate that when Si excess incorporated in the sample increases, local fluctuations of Si concentration appears and become larger with the Si content. The presence of local Si fluctuations has already been demonstrated on undoped silicon-enriched silica (SiO_X), for a silicon excess of about 25–30% [12,13]. The presence of crystallized Si-ncs has been evidenced by HRTEM since 900°C (not presented here). In addition, it has been also highlighted that, for high concentrations, rare earth ions may also exhibit inhomogeneity upon deposition [14]. Moreover, as proposed by the mixture model [15] and recently evidenced by XPS [16], oxygen can be in homogenously distributed in SRSO layers, thus leading to the formation of Oxygen-rich and Oxygen-poor network. Therefore, we can assume that both Si excess and Er content promote the separation of these two oxygen networks as highlighted in Fig. 1.

Thus, an important correlated effect of Si excess on the spatial distributions of both Si and Er atoms during deposition of the layers is clearly demonstrated. To explain this observation, we suggest that i) an inhomogeneous growth occurs which can be induced by the surface mobility of the high Si excess at 500°C (fabrication temperature), ii) Si atoms in excess and Er^{3+} ions tend to aggregate in the way of compositional fluctuation to minimize the energy of the system. As the elaboration temperature is low, we exclude the ignition of the phase separation process between Si and SiO_2 to explain these fluctuations. Si clustering is generally observed at least for an annealing temperature at 900°C [17–19]. Thus, two types of phase can be developed within the layers: areas rich in silicon and erbium and poorer ones (containing low Si excess) closer to SiO_2. The confirmation of this hypothesis would require a more in-depth study of the influence of the deposition temperature and the Si excess on the homogeneity of the elements in the layers. The loss of luminescence of Er ions in Er-doped SiO_X materials at high temperature (>1000°C) has been very frequently observed in the literature [17,20]. This quenching is generally attributed to the precipitation of Er ions and the formation of phases such as erbium oxides [7]. Accordingly, an understanding of luminescence requires the control of the structural evolution. However, the study of the nanoscale structure of these systems has only been slightly studied [8,21,22] and consequently the precipitation mechanism of the Er ions in SRSO remains very poorly understood. Hence, our samples were subjected to 1 h heat treatment at 1100°C, a temperature for which Si-ncs in silica should be formed [12] and thus be able to sensitize efficiently the Er ions [17].

3.2. Clusters analysis

The three dimensional reconstructions of the analyzed volumes by APT after annealing at 1100°C of the samples $Si_{4\%}$, $Si_{9\%}$, and $Si_{16\%}$ are presented in Fig. 2a), 2.b) and 2.c) respectively. On these volumes, we present the mapping of all the atoms of Er and only Si-ncs after their identification through cluster identification algorithm based on concentration threshold criteria. For all samples, pure Si-ncs (red) and Er-rich nanoclusters (Er-ncs) (black) are clearly observable. We can directly evidence that annealing at 1100°C during 1 h induces the diffusion and the precipitation of all Si atoms in excess and a part of Er ions. The observed nanostructure is very similar to that observed in Ce-doped $SiO_{1.5}$ thin films [14,23].

In addition, 3D reconstructions reveal the presence of two kinds of Si-ncs: isolated one and Si-ncs in the immediate vicinity of Er-ncs (Fig. 2d–f). Table 2 indicates the total density of Si-ncs and the proportion of isolated or joined ones for the three samples.

We note that the proportion of the Si-ncs joined to those rich in Er is almost identical (≈45%) for samples $Si_{4\%}$ and $Si_{9\%}$ and is more important for sample $Si_{16\%}$ (≈64%). We therefore reveal that the two samples $Si_{4\%}$ and $Si_{16\%}$ containing almost the same Er content consist of a different Si-ncs density and percentage of each kind caused by the difference of the Si excess in these two samples. For the same Er content, higher the Si excess is, fewer formed Si free nanoclusters are. We note that this evolution is clearly different from undoped SRSO materials where it is classically admitted that the density increases with the silicon excess. This can be explained by the initial, non-annealed, state of sample $Si_{16\%}$, where Si-Er-O areas are initially formed during deposition (Fig. 1c). Thus less

Table 1
Measurements of the overall composition of the analyzed samples obtained from atom probe tomography experiments.

Sample	Element (at.%)			Si excess (%)
	Si	O	Er	
$Si_{4\%}$	35.1 ± 0.4	63.1 ± 0.4	1.8 ± 0.4	3.6
$Si_{9\%}$	38.6 ± 0.5	60.1 ± 0.4	1.3 ± 0.6	8.7
$Si_{16\%}$	43.2 ± 0.4	57.9 ± 0.4	1.9 ± 0.5	16.1

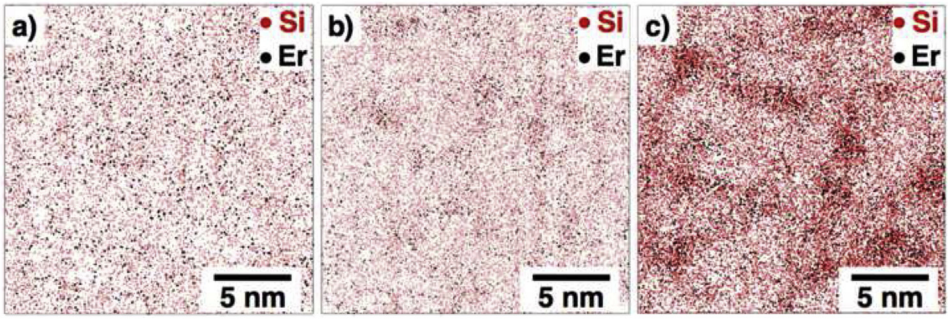

Fig. 1. Cartography of Si (red) and Er atoms (black) obtained from APT analyses of as-grown samples a) $Si_{4\%}$, b) $Si_{9\%}$ and c) $Si_{16\%}$. (For interpretation of the references to colour in this figure legend, the reader is referred to the Web version of this article.)

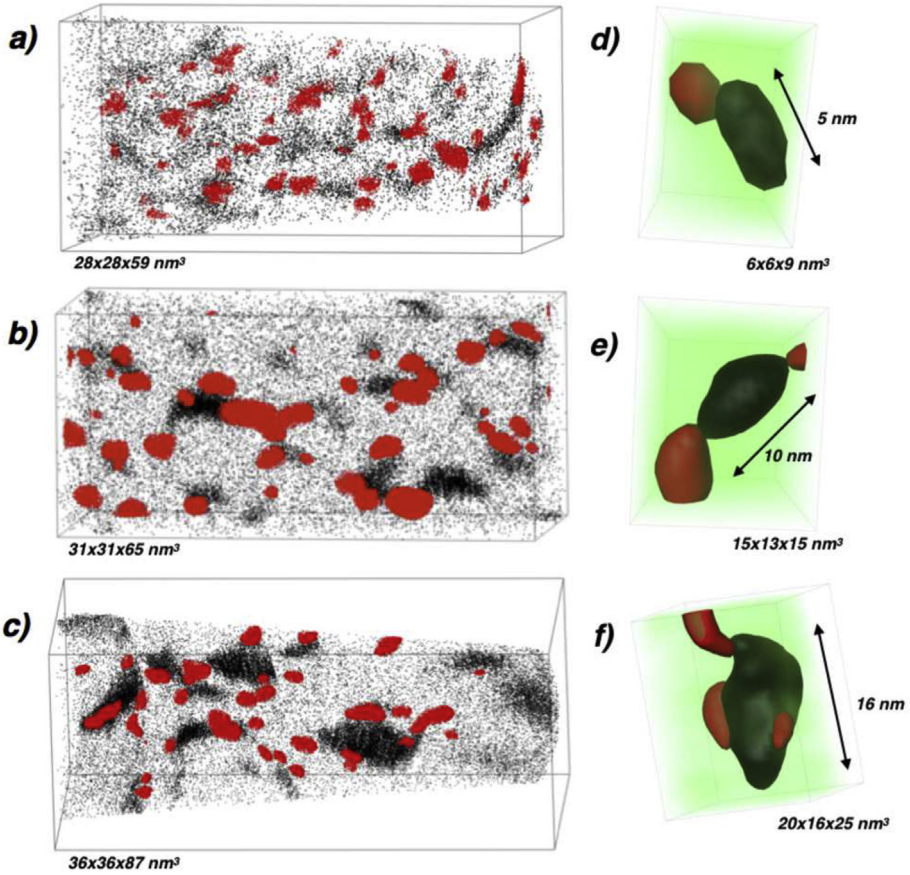

Fig. 2. 3D APT reconstruction volumes obtained on samples a) $Si_{4\%}$, b) $Si_{9\%}$ and c) $Si_{16\%}$ after annealing 1 h at 1100°C and representation of the size effect of Er-rich clusters (black) on Si-ncs (red) d, e and f. (For interpretation of the references to colour in this figure legend, the reader is referred to the Web version of this article.)

Table 2
Density and proportion of isolated and joined Si-ncs in sample $Si_{4\%}$, $Si_{9\%}$ and $Si_{16\%}$ after annealing 1 h at 1100°C.

Sample	Density of Si-ncs ($x10^{18}.cm^{-3}$)	% of isolated Si-ncs	% of joined Si-ncs
$Si_{4\%}$	3.1 ± 0.2	55%	45%
$Si_{9\%}$	0.8 ± 0.6	55%	45%
$Si_{16\%}$	1.2 ± 0.6	36%	64%

isolated Si excess in silica matrix is available to form Si nanoclusters. Moreover, the formation of these later can also be linked to the Er concentration. Indeed, sample $Si_{9\%}$ containing same population of the Si-ncs as sample $Si_{4\%}$, although it contains a higher excess of Si. This can be explained by the low Er concentration in sample $Si_{9\%}$. The effect of the dopant concentration on the Si-ncs growth and properties (size, density, isolated or joined) has already been observed in the case of Ce doped $SiO_{1.5}$ thin films [24]. Particularly striking examples of Si-ncs in immediate vicinity of Er-ncs are shown in Fig. 2d–f, which represent the effect of Er-rich

particles size on the segregation of Si-ncs. For small Er-ncs (Fig. 2d), a single Si-ncs is found on the surface whereas for bigger sizes a group of two or more Si-ncs is apparently distributed around the boundary of a single Er-ncs (Fig. 2e and f). This is strongly related to the surface tensions of the nanoclusters as well as to the minimization of their energy. This kind of nanostructure is known in the literature as Janus nanoparticles [25,26]. We recently demonstrated their formation in a similar system Ce-doped $SiO_{1.5}$ [26]. This is a critical observation that will lead us to ask whether the formation of this type of nanostructure is identical for all rare earth ions in SiO_X.

In order to obtain a better insight of the nanostructural evolution of the samples, composition measurements are required. To determine the composition of the Er-ncs quantitatively, a small box of 1 nm^3 is placed in the core of each cluster. By counting the number of atoms of each species in the sampling box, we are able to identify the composition of the Er-rich nanoparticles. The resulting compositional measurements are listed in Table 3. These particles do not correspond to a definite and stable phase in the sample $Si_{4\%}$ and $Si_{9\%}$. The only stable compound is obtained for the sample $Si_{16\%}$, containing the largest Si excess. An erbium disilicate of stoichiometry $Er_2Si_2O_7$ is evidently identified. However, APT does not allow to confirm the crystallinity nor the polymorph of the detected Er disilicate phase. Thus, further analyses are necessary to determine exactly the crystallographic nature of this phase as well as its optical properties. Note that these issues are out of the scope of this contribution. The phase transformation and the formation of Er disilicate and pure Si-ncs are surprisingly identical to those observed in the case of Ce-doped $SiO_{1.5}$ [14,24]. This important result demonstrates similar phase transformation characteristics for two different rare earths in silicon-enriched silica. Note that Er-doped and Ce-doped layers were produced by different techniques and were submitted to different annealing atmospheres.

Moreover, in all the samples, the matrix is composed of SiO_2 with diluted Er atoms. The atomic fraction of Er atoms diluted in the matrix and those constituting the precipitates have been extracted from APT analysis. The atomic fraction of the Er atoms in the matrix after annealing for the sample $Si_{4\%}$, $Si_{9\%}$ and $Si_{16\%}$ is respectively 9×10^{20} at cm^{-3}, 4×10^{20} at cm^{-3} and 7×10^{20} at cm^{-3}. The Er content in the matrix, for all samples is above the solubility limit of Er atoms in SiO_2 estimated to 0.1 at.% (7×10^{19} at cm^{-3}) [6]. This indicates that after annealing 1 h at 1100°C, the thermodynamic equilibrium may not be yet reached. The atomic fraction of Er in Er-ncs is 30%, 36% and 49% for sample $Si_{4\%}$, $Si_{9\%}$ and $Si_{16\%}$, respectively, indicating an increase of the relative quantity of Er included in the Er-rich phase with the silicon excess. However, the comparison of the samples $Si_{4\%}$ and $Si_{16\%}$ containing the same Er concentration, evidences a more advanced state of precipitation of Er ions in the later than in the former. This observation can be correlated with the initial microstructure of the as-grown layer (Fig. 1a and c). Indeed, we have shown previously that the $Si_{16\%}$ sample already exhibited a high inhomogeneity of Si and Er atoms while the $Si_{4\%}$ sample exhibited a random distribution. Thus we can conclude that the final state (after annealing) of the system depends strongly on the initial state (as-grown). More initial state presents inhomogeneity of Er and Si, the more rapidly formation of stable compound such as erbium silicate and silicon-ncs will take place because this heterogeneity can act as seeds and accelerates diffusion and phase transformation.

Table 3
Measurements of the Er-ncs composition of the analyzed samples obtained from atom probe tomography experiments after annealing 1 h at 1100°C.

Sample	Element (at.%)			Stable compound
	Si	O	Er	
$Si_{4\%}$	28.4 ± 0.4	59.7 ± 0.4	11.9 ± 0.4	None
$Si_{9\%}$	20.2 ± 0.3	66.5 ± 0.3	13.3 ± 0.3	None
$Si_{16\%}$	17.9 ± 0.4	64.7 ± 0.4	17.4 ± 0.4	$Er_2Si_2O_7$

Fig. 3 compares the evolution of the numerical density and the mean diameter of i) whole Si and Er nanoparticles (Fig. 3 a) and ii) joined and isolated Si-ncs separately (Fig. 3 b) for the three analyzed samples annealed at 1100°C. These two quantities (density and diameter) are changing from one sample to another and it is obviously related to the different Si excess and Er content. First, by increasing Si excess, a continuous decrease of the Er-ncs density is observed while their mean diameter increases. For constant Er content but different Si excess (sample $Si_{4\%}$ and $Si_{16\%}$), density of both ncs is higher but their mean diameter is smaller for layers containing a low Si excess. Secondly, we can notice that the influence of Si excess does not act identically on joined and isolated Si-ncs (Fig. 3 b). The mean diameter of joined Si-ncs continuously increases with the silicon excess while isolated Si-ncs diameter can be considered as constant for the three samples. Moreover, we note that the density ratio between isolated and joined Si-ncs slightly evolves with a decrease of the percentage of isolated ones. Such evolution on the numerical density and on the mean diameter of the particles is directly related to the initial distribution of atoms (Fig. 1) and to the formation of Er-disilicates phases (Fig. 2). Higher the Er concentration, higher is the quantity of Si that will be consumed to form a stable Er-silicate phase. Consequently, the quantity of Si atoms in excess available to form isolated Si-ncs will be lower.

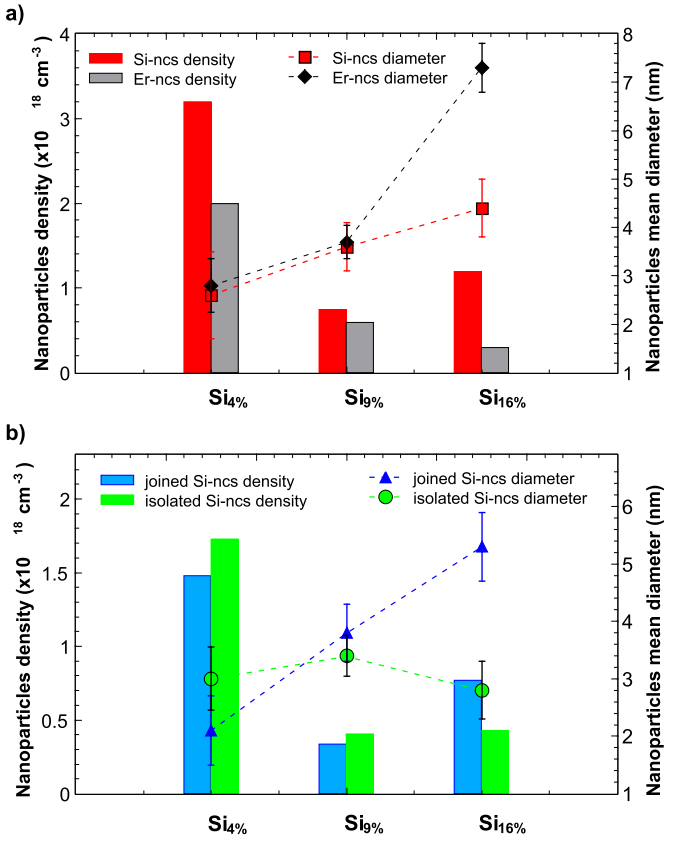

Fig. 3. a) Whole Si and Er nanoparticles density (left Y-axis) and mean diameter (right Y-axis) and b) Joined and isolated Si-ncs density (left Y-axis) and mean diameter (right Y-axis) for sample $Si_{4\%}$, $Si_{9\%}$ and $Si_{16\%}$ after 1 h annealing at 1100°C.

3.3. Photoluminescence analysis

Finally, the optical response of the sample $Si_{4\%}$, $Si_{9\%}$ and $Si_{16\%}$ annealed at 1100°C has been investigated by photoluminescence measurements. For all samples, no signal of Er^{3+} ions at 1.54 μm has been detected, evidencing a quenching of the luminescence as usually observed for high doping level of silicon rich silica and high temperature annealing [8,17,21]. Fig. 4 shows the PL spectra in the range of 550–1000 m, which is typical of Si-ncs emission. This result is in agreement with the APT ones revealing the presence of Si-ncs in our samples. The PL efficiency is maximum for sample $Si_{16\%}$ and at least two times more intense than samples $Si_{4\%}$ and $Si_{9\%}$ which present similar luminescence. Moreover, we have previously shown that the mean diameter of Si-ncs (Fig. 3 a) increases from 2.6 nm to 4.4 nm by increasing the Si excess. Such a raise of the Si-ncs diameter with the Si excess should be evidenced on the emission properties by a red shift of the PL peaks which it is not observed in our case. As mentioned previously, Si-ncs can be divided in two classes: i) Si-ncs isolated in the matrix; ii) Si-ncs joined to Er-rich particles (Fig. 2d, e and f). The diameter of isolated Si-ncs for sample $Si_{4\%}$, $Si_{9\%}$ and $Si_{16\%}$ can be considered as constant (Fig. 3 b) and are compatible with the constant PL peak position under the hypothesis that only isolated Si-ncs are responsible of the PL emission as previously demonstrated on Ce-doped $SiO_{1.5}$ system [24]. In this case, the authors evidenced a luminescence quenching of Si-ncs in the vicinity of rare-earth silicate particles and attributed the optical emission to only isolated Si-ncs.

4. Conclusions

In conclusion, the use of atom probe tomography combined with photoluminescence experiments allowed us to identify the origin of the emission properties of Er-doped silicon nanoclusters in silica. First, these results show an important effect of the silicon excess and Er concentration on the nanoscale structure and phase present in Er doped SiO_X thin layers. This is an important point to discuss. Indeed, the studies carried out on this system during last years had the aim of forming Si nanoparticles in the Er doped silica in order to improve the emission efficiency of the Er ions.

However, our observations have shown that the nanoscale structure in this system interacts strongly with the amount of silicon excess or the Er content. Therefore, the Si excess atoms will interact with the Er ions to form a mixed compound rather than pure Si nanoparticles in a conventional manner. Moreover, we demonstrated the formation of Er-silicate compound in such system, in contrary to what has been mentioned in the literature that an Er-oxide phase tends to be formed at high annealing temperature (>1100–1200°C). On the other hand, we highlighted a complex interaction between Si, Er and O atoms leading to the formation of an original configuration of erbium clusters in the proximity to Si-ncs. Furthermore, the correlation between APT and PL experiments has allowed us to diagnose deeply the origin of the optical response in such system. Particularly, the major contribution of isolated silicon nanoparticles, as well as the explanation of Er^{3+} luminescence quenching under indirect excitation, as it is widely observed in the literature, due to the growth of Er-rich phases. The latter has a detrimental effect on the energy transfer and thus further work is required to fully explore the nanoscale structure of such system.

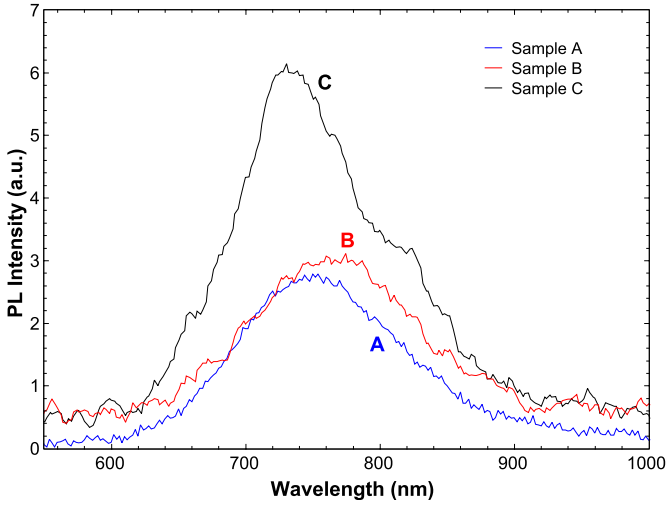

Fig. 4. Photoluminescence spectra of the sample $Si_{4\%}$, $Si_{9\%}$ and $Si_{16\%}$ annealed at 1100°C in the spectral range 550–1000 nm.

Acknowledgments

One of the author (G. Beainy) acknowledges the financial support from "Région Haute-Normandie".

References

[1] A. Polman, Erbium implanted thin film photonic materials, J. Appl. Phys. 82 (1997) 1.
[2] P.G. Kik, M.L. Brongersma, A. Polman, Strong exciton-erbium coupling in si nanocrystal-doped sio_2, Appl. Phys. Lett. 76 (2000) 2325.
[3] M. Fujii, M. Yoshida, Y. Kanzawa, S. Hayashi, K. Yamamoto, 1.54 μm photoluminescence of er^{3+} doped into sio2 films containing si nanocrystals: evidence for energy transfer from si nanocrystals to er^{3+}, Appl. Phys. Lett. 71 (1997) 1198.
[4] G. Franzò, V. Vinciguerra, F. Priolo, The excitation mechanism of rare-earth ions in silicon nanocrystals, Appl. Phys. A 69 (1999) 3.
[5] G. Franzò, S. Boninelli, D. Pacifici, F. Priolo, F. Iacona, C. Bongiorno, Sensitizing properties of amorphous si clusters on the 1.54-μm luminescence of er in si-rich sio_2, Appl. Phys. Lett. 82 (2003) 3871.
[6] M.W. Sckerl, S. Guldberg-Kjaer, M.R. Poulsen, P. Shi, J. Chevallier, Precipitate coarsening and self organization in erbium-doped silica, Phys. Rev. B 59 (1999) 13494.
[7] A. Thogersen, J. Mayndi, L. Vines, M. Sunding, A. Olsen, S. Diplas, M. Mitome, Y. Bando, The formation of er-oxide nanoclusters in sio_2 thin films with excess si, J. Appl. Phys. 106 (2009), 014305.
[8] P. Pellegrino, B. Garrido, J. Arbiol, C. Garcia, Y. Lebour, J.R. Morante, Site of er ions in silica layers codoped with si nanoclusters and er, Appl. Phys. Lett. 88 (2006), 121915.
[9] K. Hijazi, R. Rizk, J. Cardin, L. Khomenkova, F. Gourbilleau, Towards an optimum coupling between er ions and si-based sensitizers for integrated active photonics, J. Appl. Phys. 106 (2009), 024311.
[10] W. Lefebvre-Ulrikson, F. Vurpillot, X. Sauvage (Eds.), Atom Probe Tomography, Academic Press, 2016.
[11] M. Thuvander, H.-O. Andren, K. Stiller, Q.-H. Hu, A statistical method to detect ordering and phase separation by apfim, Ultramicroscopy 73 (1998) 279.
[12] M. Roussel, E. Talbot, C. Pareige, R.P. Nalini, F. Gourbilleau, P. Pareige, Confined phase separation in sio_x nanometric thin layers, Appl. Phys. Lett. 103 (2013), 203109.
[13] M. Roussel, E. Talbot, P. Pareige, F. Gourbilleau, Influence of the supersaturation on si diffusion and growth of si nanoparticles in silicon-rich silica, J. Appl. Phys. 113 (2013), 063519.
[14] G. Beainy, J. Weimmerskirch-Aubatin, M. Stoffel, M. Vergnat, H. Rinnert, C. Castro, P. Pareige, E. Talbot, Structural and optical study of ce segregation in ce-doped $sio_{1.5}$ thin films, J. Appl. Phys. 118 (2015) 234308.
[15] F.G. Bell, L. Ley, Photoemission study of $sio_x(0\leq x\leq 2)$ alloys, Phys. Rev. B 37 (1988) 8383–8393.
[16] D. Risti, M. Ivanda, G. Speranza, Z. Siketi, I. Bogdanovi-Radovi, M. Marciu, M. Risti, O. Gamulin, S. Musi, K. Furi, G.C. Righini, M. Ferrari, J. Phys. Chem. C 116 (18) (2012) 10039–10047.
[17] F. Gourbilleau, M. Levalois, C. Dufour, J. Vicens, R. Rizk, Optimized conditions for an enhanced coupling rate between er ions and si nanoclusters for an improved 1.54-μm emission, J. Appl. Phys. 95 (2004) 3717.
[18] F. Iacona, C. bongiorno, C. Spinella, S. Boninelli, F. Priolo, Formation and evolution of luminescent si nanoclusters produced by thermal annealing of sio_x films, J. Appl. Phys. 95 (2004) 3723.
[19] E. Talbot, R. Lardé, F. Gourbilleau, C. Dufour, P. Pareige, Si nanoparticles in sio_2 an atomic scale observation for optimization of optical devices, Eur. Phys. Lett. 87 (2009) 26004.

[20] L.-F. Bian, C.G. Zhang, W.D. Chen, C.C. Hsu, T. Shi, Local environment of er^{3+} in er-doped si nanoclusters embedded in sio_2 films, Appl. Phys. Lett. 89 (2006) 231927.
[21] E. Talbot, R. Lardé, P. Pareige, L. Khomenkova, K. Hijazi, F. Gourbilleau, Nanoscale evidence of erbium clustering in er-doped silicon-rich silica, Nanoscale Res. Lett. 8 (2013) 39.
[22] A. Eljarrat, L. Lopez-Conesa, J. Rebled, Y. Berencen, J. Ramirez, B. Garrido, C. Magen, S. Estrade, F. Peiro, Structural and compositional properties of er-doped silicon nanoclusters/oxides for multilayered photonic devices studied by stem-eels, Nanoscale 5 (2013) 9963.
[23] J. Weimmerskirch-Aubatin, M. Stoffel, X. Devaux, A. Bouché, G. Beainy, E. Talbot, P. Pareige, Y. Fagot-Révurat, M. Vergnat, H. Rinnert, Observation of a nanoscale phase separation in blue-emitting ce-doped $sio_{1.5}$ thin films, J. Mater. Chem. C 3 (2015) 12499.
[24] G. Beainy, J. Weimmerskirch-Aubatin, M. Stoffel, M. Vergnat, H. Rinnert, P. Pareige, E. Talbot, Correlation between the nanoscale structure and the optical properties of ce-doped $sio_{1.5}$ thin films, J. Lumin. 191 (2017) 88.
[25] M. Lattuada, T. Hatton, Synthesis, properties and applications of janus nanoparticles, Nano Today 6 (2011) 286.
[26] G. Beainy, J. Weimmerskirch-Aubatin, M. Stoffel, M. Vergnat, H. Rinnert, P. Pareige, E. Talbot, Direct insight into ce-silicates/si-nanoclusters snowman-like janus nanoparticles formation in ce-doped sio_X thin layers, J. Phys. Chem. C 121 (2017) 12447.